Available online at www.sciencedirect.com
SCIENCE DIRECT
Journal of Molecular Catalysis A: Chemical 241 (2005) 118–125
JOURNAL OF MOLECULAR CATALYSIS A: CHEMICAL
www.elsevier.com/locate/molcata

TS-1 loaded with sulfated zirconia as bifunctional oxidative and acidic catalyst for transformation of 1-octene to 1,2-octanediol

Didik Prasetyoko [a], Zainab Ramli [a], Salasiah Endud [a], Hadi Nur [b,*]

[a] *Department of Chemistry, Faculty of Science, Universiti Teknologi Malaysia, 81310 UTM Skudai, Johor, Malaysia*
[b] *Ibnu Sina Institute for Fundamental Science Studies, Universiti Teknologi Malaysia, 81310 UTM Skudai, Johor, Malaysia*

Received 11 January 2005; received in revised form 24 June 2005; accepted 29 June 2005
Available online 15 August 2005

Abstract

Titanium silicalite (TS-1) loaded with sulfated zirconia as bifunctional oxidative and acidic catalyst has been synthesized at various loadings of zirconium (2–20 wt%). Structure and properties of the samples were characterized by X-ray diffraction (XRD), temperature programmed reduction (TPR), Fourier transform infrared (FTIR) and UV–vis diffuse reflectance (UV–vis DR) spectroscopy techniques. The monolayer dispersion capacity of zirconium on the TS-1 was found to be 0.65 Zr^{4+} nm^{-2} TS-1. The UV–vis DR spectroscopy showed that the tetrahedral coordination of the titanium was observed in all samples, while octahedral zirconium was only observed in the samples containing high amount of zirconium loading (10, 15 and 20 wt%). The TPR profiles suggested that the zirconium structure impregnated on the surface of TS-1 with high amount of zirconium loading (15 and 20 wt%) have a similar structure to sulfated zirconia calcined at 500 °C. Adsorption of pyridine onto the samples indicated that Brönsted acid sites are only present in samples with high sulfated zirconia loading, i.e. 15 and 20 wt%. As analyzed by XRD, the formation of Brönsted acid sites is due to the presence of disulfate species on the surface of TS-1. It has been demonstrated that samples with 15 and 20 wt% loadings of sulfated zirconia showed activity towards consecutive transformation of 1-octene to 1,2-octanediol through the formation of 1,2-epoxyoctane using aqueous hydrogen peroxide.

Keywords: Bifunctional catalyst; TS-1; 1-Octene; Sulfated zirconia; Epoxidation; Hydrolysis

1. Introduction

A large segment of the modern chemical industry is based on selective catalytic oxidation processes [1]. More than 60% of the chemicals and intermediates synthesized via catalytic processes are the products of oxidation. Most of the oxidation processes are being carried out in the gas and liquid phases. Catalytic oxidation in the liquid phase is widely used in bulk chemicals manufacture and are becoming increasingly important in the synthesis of fine chemicals [2]. Over the last decade, titanium silicalite (TS-1) which was first synthesized by Taramasso et al. [3] in 1983 has shown excellent catalytic activity in organic oxidation reactions using hydrogen peroxide as oxidant under mild conditions. In alkenes epoxidation, many works have been done to enhance the epoxide selectivity due to the industrial importance of epoxides in the synthesis of organic and pharmaceutical materials. The ability of TS-1 to catalyze a wide variety of oxidation transformations including alkenes epoxidation with 30% aqueous hydrogen peroxide has led to extensive research worldwide on the synthesis of related heterogeneous catalysts for liquid-phase oxidation [4]. The major side product of the epoxidation reaction using H_2O_2 is diols. It has been known that the formation of diols from epoxides is catalyzed by Brönsted acid sites. On the other hand, diols are attractive feedstocks for the fine chemical industry. At present, diols are manufactured industrially via a two-step sequence consisting of epoxidation of an olefin, followed by hydrolysis of the resulting epoxides.

Much attention has been paid to sulfated zirconia recently due to its significant catalytic activity in many hydrocarbon

* Corresponding author. Tel.: +607 5536061; fax: +607 5536080.
E-mail address: hadi@kimia.fs.utm.my (H. Nur).

1381-1169/$ – see front matter © 2005 Elsevier B.V. All rights reserved.
doi:10.1016/j.molcata.2005.06.070

conversions, such as isomerization, alkylation, acylation, esterification, etherification, condensation, nitration and cyclization [5–9]. It was shown that the catalytic activity of the sulfated zirconia is related mainly to its acid properties. Some authors have reported that the catalysts contain both Brönsted and Lewis acid sites which are responsible for the activity. Several studies have been done on the structure and activity of zirconia-loaded silica, alumina and mesoporous molecular sieves [10–15]. However, the preparation of sulfated zirconia loaded on a strong oxidative support as bifunctional oxidative and acidic catalyst, for the consecutive reaction of alkenes to diols through the formation of epoxides have never been reported. In this study, TS-1 loaded with sulfated zirconia has been synthesized and used as bifunctional oxidative and acidic catalyst in which the Ti atoms in TS-1 acts as oxidative acid sites while sulfated zirconia deposited on the surface of TS-1 acts as Brönsted acid sites. The effect of zirconium loading on the structure and properties of the catalysts was investigated. The catalytic activity was examined in the consecutive transformation of 1-octene to 1,2-octanediol through the formation of 1,2-epoxyoctane using aqueous hydrogen peroxide as oxidant.

2. Experimental

2.1. Preparation of sample

TS-1 containing 1 mol% of titanium was prepared according to a procedure described earlier [3,16]. TS-1 loaded with sulfated zirconia (SZ) was prepared by the wet impregnation method. The TS-1 was added into a solution of zirconium sulfate hydrate [$Zr(SO_4)_2{\cdot}4H_2O$] in water. The mixture was stirred at room temperature for 3 h, followed by evaporation of the solvent at 100 °C. The solid was dried at 100 °C for 24 h and calcined at 500 °C for 7 h. The resulting sample was denoted as *X*SZ/TS-1, in which *X* is the percentage of zirconium in the sample. For control, bare sulfated zirconia (SZ500) was prepared by drying of $Zr(SO_4)_2{\cdot}4H_2O$ at 100 °C for 3 days followed by calcination at 500 °C for 7 h. Table 1 summarizes the zirconium contents of the samples and their treatment after impregnation with $Zr(SO_4)_2$.

Table 1
Zirconium content of the samples[a]

Sample	Zr (wt%)
TS-1	0[b]
2SZ/TS-1	1.8[c]
5SZ/TS-1	5.1[c]
10SZ/TS-1	9.9[c]
15SZ/TS-1	15.5[c]
20SZ/TS-1	20.3[c]

[a] After the impregnation of $Zr(SO_4)_2$, the sample was dried at 100 °C for 24 h and calcined.
[b] The sample was calcined at 550 °C for 5 h.
[c] The sample was calcined at 500 °C for 7 h.

2.2. Characterization

All samples were characterized by powder X-ray diffraction (XRD) for crystallinity and phase content of the solid materials, using a Bruker Advance D8 difractometer with the Cu Kα (λ = 1.5405 Å) radiation as the diffracted monochromatic beam at 40 kV and 40 mA. The pattern was scanned in the 2θ ranges between 20° and 40° at a step 0.020° and step time 1 s. UV–vis DR spectra were recorded under ambient conditions using a Perkin-Elmer Lambda 900 UV/VIS/NIR spectrometer. The spectra were monitored in the range of 190–600 nm. Temperature programmed reduction (TPR) experiments were performed using a TPDRO 1100 Thermo Quest CE instrument. The sample (0.05 g) was pre-treated in a nitrogen flow at the rate of 30 ml min^{-1} at 500 °C for 1 h and cooled down to 100 °C. The reduction analysis was performed by heating the sample from 100 up to 900 °C at a rate of 10 °C min^{-1} in a flowing mixture of 5% hydrogen in nitrogen H_2/N_2 at the rate of 25 ml min^{-1}. Infrared (IR) spectra of the samples were collected on a Shimadzu Fourier Transform Infrared (FTIR) spectrometer, with a spectral resolution of 2 cm^{-1}, scans 10 s, at temperature 20 °C. For acidity evaluation, the wafer of the sample (10–12 mg) was prepared and locked in the cell equipped with CaF_2 windows and evacuated at 400 °C under vacuum condition for 4 h. Infrared spectra of the sample were recorded at room temperature in the hydroxyl region of 4000–3000 cm^{-1} and pyridine vibration region at 1700–1300 cm^{-1}.

2.3. Catalytic testing

The catalyst performance was tested in the epoxidation of 1-octene using aqueous H_2O_2 (30%) as oxidant. The reaction mixture containing 1-octene (8 mmol), H_2O_2 (15 mmol) and acetone (10 g) as solvent was put in a round bottom flask equipped with a condenser. The catalyst (0.05 g) was then added to the solution. The reaction was carried out in an oil bath under stirring at 70 °C. The products of the reaction were analyzed by a Hewlett-Packard 6890 N gas chromatograph using an Ultra-1 column and a Hewlett-Packard GC-MSD instrument using an HP5 column.

3. Results and discussion

3.1. X-ray diffraction

Fig. 1 shows the XRD patterns of the SZ500 and SZ/TS-1 samples. It is shown that no diffraction lines for tetragonal or monoclinic phases of zirconia are observed indicating that the SZ is highly dispersed on the surface of TS-1. It is found that the MFI structure of TS-1 was maintained after the sulfated zirconia (SZ) loading. However, the XRD peak intensities of TS-1 decreased when the loading amount of the SZ was increased. This might be due to the decrease in the percentage

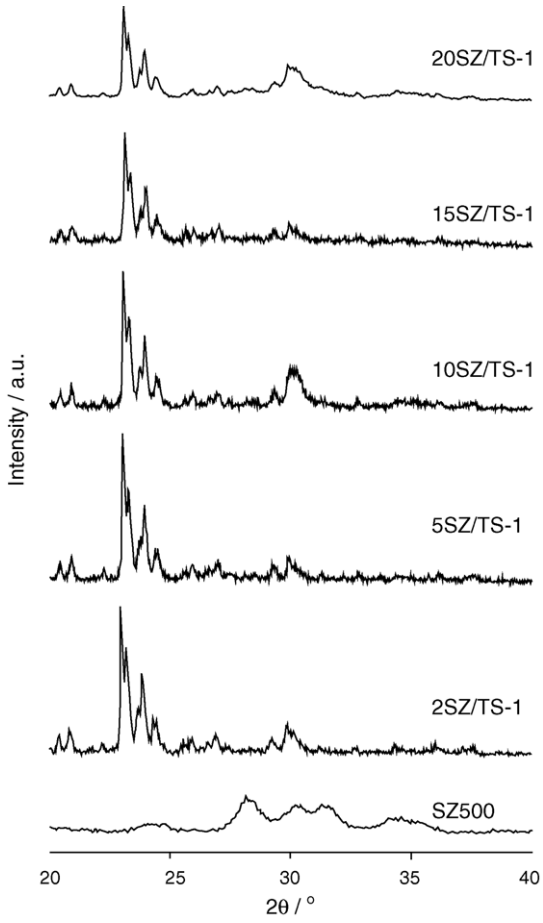

Fig. 1. XRD pattern of the TS-1 loaded with sulfated zirconia.

amount of TS-1 in the samples as the loading amount of the SZ increased.

The monolayer coverage of ZrO_2 can be determined from the plot of the diffraction line intensity of TS-1 at $2\theta = 23^\circ$ versus loading amount of zirconium on the samples as shown in Fig. 2. The diffraction line intensities of 2SZ/TS-1 and 5SZ/TS-1 were similar to those of the parent TS-1 and are significantly lower for 10SZ/TS-1, 15SZ/TS-1 and 20SZ/TS-1. Hence, a horizontal line was found for low SZ loadings and another straight line with a tangent can be drawn for higher SZ loadings. The interception of the two lines was found at 6 wt% of SZ loading which is equal to 0.65 Zr^{4+} nm^{-2} TS-1. This value corresponds to monolayer dispersion capacity of zirconium on the TS-1.

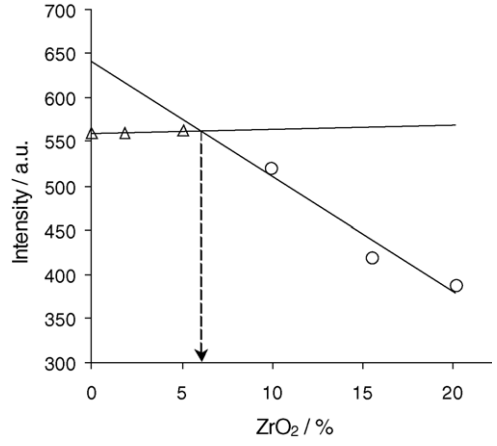

Fig. 2. The graph of peak intensity of TS-1 at $2\theta = 23^\circ$ vs. loading amount of zirconium on the s TS-1 loaded with sulfated zirconia.

3.2. Infrared spectroscopy

The infrared spectra of zeolite lattice vibration between 1400 and 400 cm^{-1} are depicted in Fig. 3. According to Flanigen [17], the absorption bands at around 1100, 800 and 450 cm^{-1} are lattice modes associated with internal linkages in SiO_4 (or AlO_4) tetrahedral and are insensitive to structural changes. The absorption bands at around 1230 and 547 cm^{-1} are characteristic of the MFI type zeolite structure and are sensitive to structure changes. All samples showed a band at around 970 cm^{-1}. The vibrational modes at around this frequency may be the result of several contributions, i.e. the asymmetric stretching modes of Si–O–Ti linkages, terminal Si–O stretching of SiOH–(HO)Ti "defective sites" and titanyl [Ti=O] vibrations. However, this band can be attributed to the titanium in the framework, since silicalite,

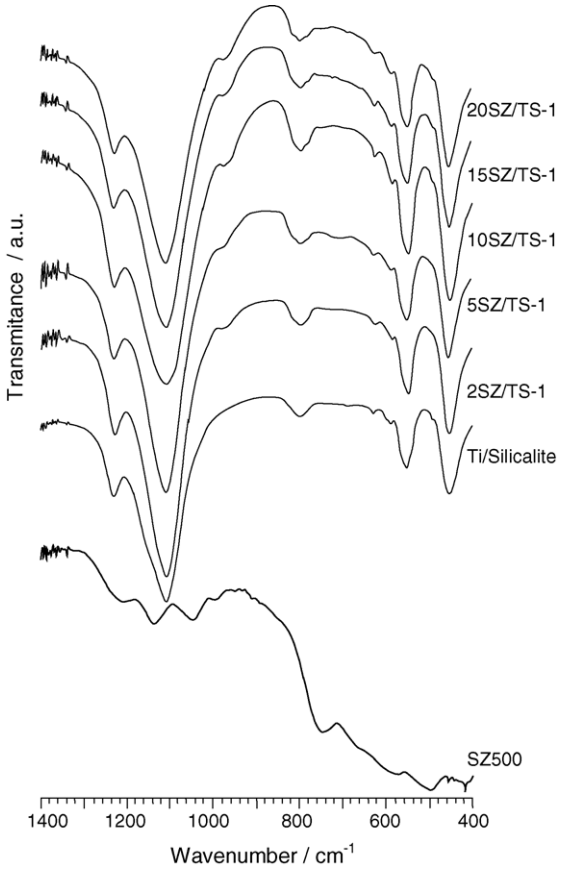

Fig. 3. Infrared spectra of TS-1 loaded with sulfated zirconia.

a Ti-free zeolite, did not show any band at around this frequency [18–21]. In addition, impregnation of silicalite with Ti (sample Ti/silicalite) gave rise to no band around 970 cm^{-1}. Therefore, it is concluded that the TS-1 sample contains Si–O–Ti connections. There is no band shifting or additional band observed after impregnation of zirconium sulfate on TS-1. This finding suggests that both the MFI structure and titanium framework were still maintained after loading of SZ.

3.3. UV–vis diffuse reflectance spectroscopy

As shown in Fig. 4, an absorption band at around 210 nm was observed in the spectra of SZ/TS-1. This band is attributed to ligand-to-metal charge transfer not only associated with isolated Ti^{4+} framework sites (between O^{2-} and the central Ti(IV) atoms) in tetrahedral coordination but also with isolated Zr^{4+}. This is supported by the fact that the impregnation of HZSM-5, a Ti-free aluminosilicalite, with zirconium sulfate (5SZ/HZSM-5) also showed a band at around 210 nm. The second band at lower energy of about 230 nm is attributed to zirconium species in an octahedral coordination [3,22].

Fig. 4 displays UV–vis DR spectra of SZ500 and SZ/TS-1 catalysts. The UV–vis DR spectrum of SZ500 indicates the existence of a shoulder band at around 210 nm and a sharp band centered at 230 nm. A single absorption band at 210 nm was observed in the spectrum of SZ/TS-1 containing low amounts of zirconium (2, 5 and 10 wt%), while a band at 225 nm was observed in the case of 15SZ/TS-1 and 20SZ/TS-1. The decrease in intensity of the band at 210 nm with an increase in SZ loading (up to 15 wt%) suggests that tetrahedral titanium species in the TS-1 was covered by SZ. This implies that as the amount of SZ loading increases, concentration of tetrahedral titanium species decreases.

Octahedral zirconium species, which corresponds to the peak at 230 nm, starts to appear in 10SZ/TS-1, being significantly high at higher SZ loading (Fig. 4). This finding indicates that not only SZ/TS-1 contains tetrahedral Ti but also agglomerated SZ at high zirconium loading.

3.4. Temperature programmed reduction

The TPR profiles for SZ500 and SZ/TS-1 after calcination at 500 °C are shown in Fig. 5. There is no peak of hydrogen consumed for sulfate-free zirconia, indicating that reduction did not occur in the sample. The SZ500 showed broad and sharp peaks with high intensities, starting at 500 °C and peaking at 700–720 °C and 750 °C. Similar TPR profiles with lower reduction temperatures can be observed for 15SZ/TS-1 and 20SZ/TS-1. The TPR profiles of 2SZ/TS-1, 5SZ/TS-1 and 10SZ/TS-1 showed a broad signal at reduction temperature of 500–700 °C. It is observed that both the signal intensity and reduction temperature decreased as SZ loading decreased.

According to Xu and Sachtler [23], the high temperature TPR peaks are assigned to the reduction of sulfate species in the sample to form sulfur dioxide and water. Besides sulfur dioxide, hydrogen sulfide was also evolved during treatment of sulfated zirconia with hydrogen in helium at high temperature [24]. Meanwhile, Bobricheva et al. [25] and Vera et al. [26] suggested that the peak at temperature range of

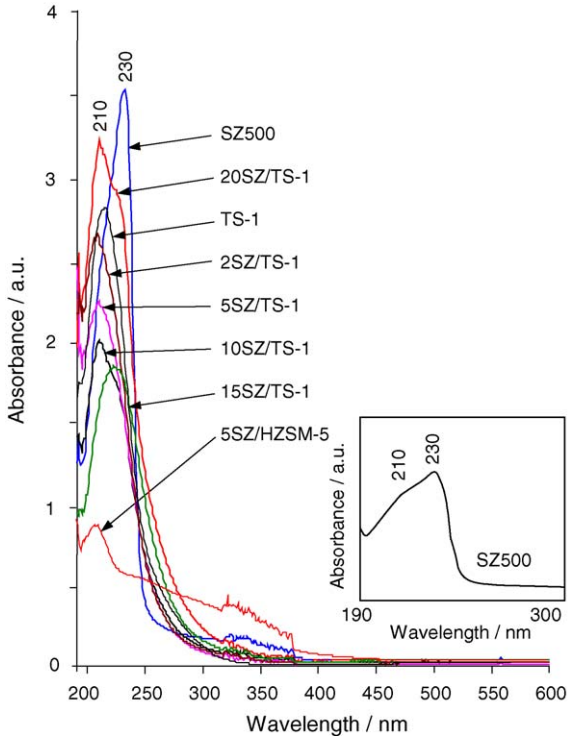

Fig. 4. UV–vis diffuse reflectance spectra of TS-1 loaded with sulfated zirconia.

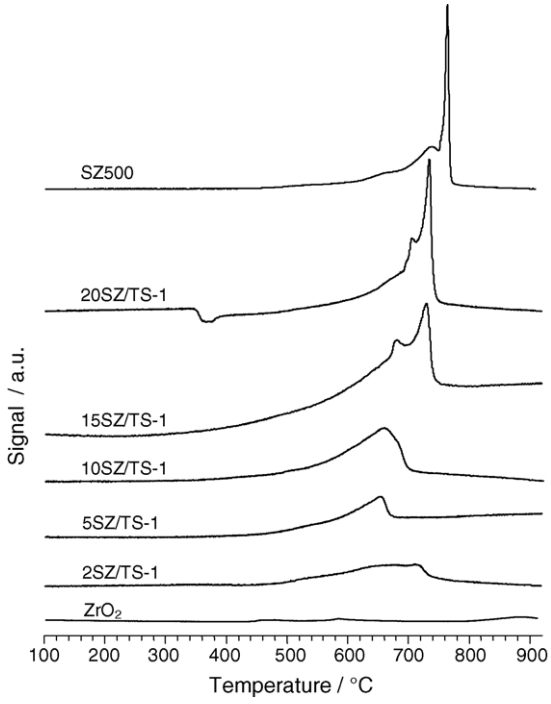

Fig. 5. TPR profiles of TS-1 loaded with sulfated zirconia.

500–600 °C is attributed to a surface process of lattice oxygen elimination (formation of anionic vacancies) and the reduction of Zr^{4+} to Zr^{3+} on the surface of zirconia sulfate during the hydrogenation process. It suggests that release of sulfate from the surface of sulfated zirconia occurs during these processes. Therefore, it can be concluded that all the TPR peaks at low and high reduction temperatures are attributed to desorption of sulfate species. Furthermore, TPR profiles of 15SZ/TS-1 and 20SZ/TS-1 are similar to those of SZ500, suggesting that there is no difference in the molecular structure of SZ between these samples.

3.5. Acidity

Fig. 6a shows the FTIR spectra of the SZ/TS-1 samples after evacuation at 400 °C for 4 h under vacuum. In the region of hydroxyl groups, the peak at 3745 cm^{-1}, which is assigned as silanol hydroxyl groups, can be clearly observed for samples with low loading amount of the SZ (2SZ/TS-1 and 5SZ/TS-1). This band was diminished at higher SZ loading (10-20SZ/TS-1), suggesting the SZ is located in the space/sites previously occupied by silanol groups. It is also possible that SZ contains hydroxyl groups since the peak at around 3550 cm^{-1} corresponds to the hydrogen bonding between the hydroxyl groups (see Fig. 9).

The FTIR spectra of the SZ/TS-1 samples in the sulfate region are shown in Fig. 6a. It is shown that the spectra of

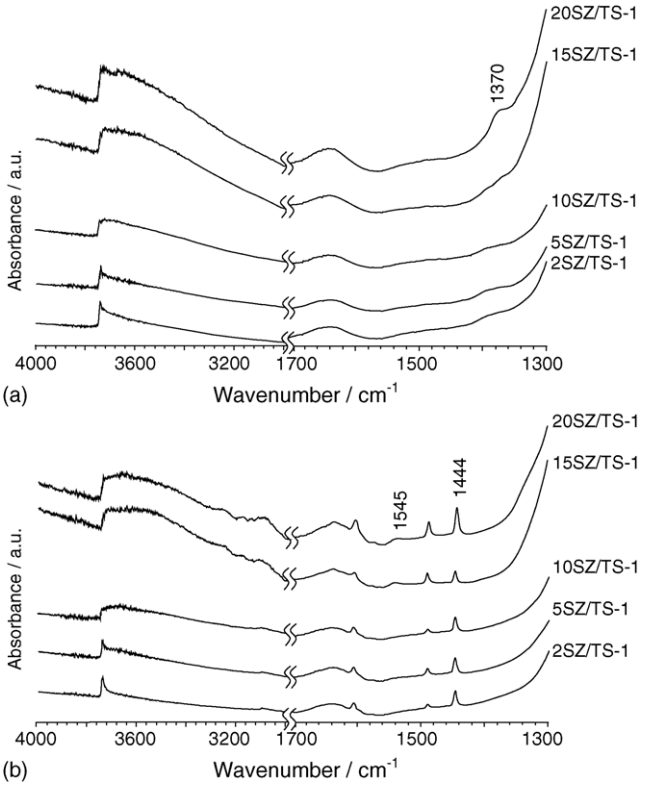

Fig. 6. FTIR spectra of the samples: (a) after evacuation at 400 °C for 4 h in vacuum, (b) after pyridine adsorption and evacuation at 150 °C for 1 h.

2SZ/TS-1, 5SZ/TS-1 and 10SZ/TS-1 are similar. The spectra of 15SZ/TS-1 and 20SZ/TS-1 showed an additional peak at 1370 cm^{-1} which is assigned to $\nu_{S=O}$ asymmetric vibration [27]. It is clearly observed that the intensity of the peak was significantly high in 20SZ/TS-1 suggesting an increase in the amount of sulfate with an increase in SZ loading.

It is interesting to relate the surface coverage obtained from XRD with the $\nu_{S=O}$ asymmetric peak at 1370 cm^{-1} which appeared on the spectra of samples. It has been calculated from the XRD data that the monolayer dispersion of zirconium is 0.65 Zr^{4+} nm^{-2} TS-1. It is revealed that the $\nu_{S=O}$ asymmetric peak only starts to appear in the spectrum of 15SZ/TS-1 although 10SZ/TS-1 has the zirconium content almost double compared to the amount of zirconium monolayer dispersion capacity calculated from the XRD data which is 1.12 Zr^{4+} nm^{-2} TS-1. It can be suggested that the $\nu_{S=O}$ asymmetric band only becomes detectable in SZ/TS-1 that contains a double layer of SZ.

The acidity of the SZ/TS-1 catalysts was monitored by FTIR using pyridine as a probe molecule (see Fig. 6b). There were no significant changes in the hydroxyl region of the spectra of the samples after pyridine adsorption compared to that before pyridine adsorption. The presence of silanol peak after pyridine adsorption indicates that the silanol groups do not react with pyridine, indicating that the silanol groups are not acidic. The peaks at 1608 and 1444 cm^{-1} in the spectra of 2SZ/TS-1, 5SZ/TS-1 and 10SZ/TS-1 are attributed to adsorbed pyridine bound coordinatively with Lewis acid sites. The spectra of 15SZ/TS-1 and 20SZ/TS-1 showed the additional absorption bands at 1640 and 1545 cm^{-1} which correspond to pyridine interacting with Brönsted acid sites. The disappearance of the $\nu_{S=O}$ asymmetric peak after the adsorption of pyridine is due to the reduction of the bond order of S=O from a highly covalent double-bond character to a lesser double–bond character; the shift of the band to a lower wavenumber was observed when a basic pyridine molecule was adsorbed on the catalysts [28].

The acidity study also indicates that SZ is responsible for the formation of Brönsted acid sites. In addition, it proves that Brönsted acid sites are present only in the samples containing double layer of zirconium, whereas samples with monolayer of zirconium do not show Brönsted acidity. Since the Brönsted acidity is only found in the sample containing octahedral zirconium (see UV–vis spectra of 15SZ/TS-1 and 20SZ-TS-1 in Fig. 4), it can be concluded that the sulfate species are bonded with octahedral zirconium and not with tetrahedral zirconium. This conclusion is supported by the model proposed by Clearfield et al. [29].

3.6. Catalytic activity

The catalytic properties of the SZ/TS-1 samples were studied in the catalytic epoxidation of 1-octene using H_2O_2 as oxidant in acetone as solvent at 70 °C. The same reactions were carried out over a mechanical mixture of TS-1 and

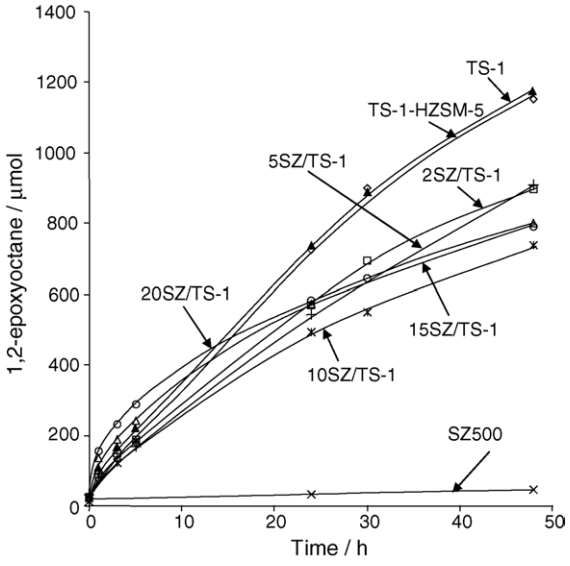

Fig. 7. The oxidation rate of 1-octene to 1,2-epoxyoctane using TS-1 loaded with sulfated zirconia with aqueous H_2O_2 as oxidant. All reactions were carried out in acetone as solvent at 70 °C.

HZSM-5 zeolite (TS-1-HZSM-5) for comparison. The amount of HZSM-5 was adjusted to match the amount of Brönsted acid in 20SZ/TS-1. As analyzed by pyridine adsorption, the concentration of Brönsted acid of HZSM-5 was 0.5 mmol g^{-1}. Theoretically, the epoxidation reaction of alkene to epoxide and the hydrolysis of epoxide to form diol are catalyzed by oxidative and acidic sites, respectively.

Fig. 7 shows the oxidation rate of 1-octene to 1,2-epoxyoctane using TS-1 loaded with sulfated zirconia using aqueous H_2O_2 as oxidant. At the beginning, the initial reaction rate of the catalysts with low zirconium loading (2SZ/TS-1, 5SZ/TS-1 and 10SZ/TS-1) was similar to that of TS-1 and TS-1-HZSM-5, whereas catalysts with high zirconium loading (15SZ/TS-1 and 20SZ/TS-1) showed considerably higher activities. However, at longer reaction time, TS-1 and TS-1-HZSM-5 showed the highest activity among the SZ/TS-1 catalysts (see Fig. 7). Meanwhile, SZ500 was totally inactive toward epoxidation. It was also observed that the catalytic activity of TS-1 was similar to that of TS-1-HZSM-5 suggesting that the epoxidation of 1-octene was not affected by HZSM-5. In order to evaluate H_2O_2 selectivity, the reaction was carried out with a similar molar amount of 1-octene and H_2O_2. It is observed that the yield of 1,2-epoxyoctane decreased with decreasing H_2O_2 after 24 h of reaction time under stirring condition compared to the system containing large excess of H_2O_2 (15 mmol) against 1-octene (8 mmol). The decrease in the molar amount of H_2O_2 and 1,2-epoxyoctane were similar (ca. 15%). This finding indicates that it is necessary to use excess amount of H_2O_2 in order to compensate the decomposition of H_2O_2 during the reaction.

As shown in Fig. 7, at the initial stage, the 15SZ/TS-1 and 20SZ/TS-1 catalysts had similar activities towards the formation of 1,2-epoxyoctane. The characterization results described in Sections 3.3 and 3.5 showed that both samples contain octahedral zirconium, sulfate species and Brönsted acid sites. In order to confirm the effect of sulfate species on enhancement of the catalytic activity, the epoxidation reaction was carried out using TS-1 containing 20 wt% of the sulfate-free zirconia. The result clearly showed that its reaction rate is similar to that of TS-1. Addition of HZSM-5, an acid catalyst, also shows insignificant change in the reaction rate. The structure of zirconium species present in the samples did not influence the catalytic activity of the parent catalyst either, since SZ500 is inactive as catalyst. Based on the above considerations, one concludes that enhancement of the epoxidation activity is not affected by the presence of the double layer of zirconium, the Brönsted acid sites or the octahedral zirconium. This suggests that the enhancement of the catalytic activity at the initial reaction rate could be attributed to the sulfate-bonded zirconia species present on the surface of TS-1 loaded with high amount of sulfated zirconia. The possible explanation for this phenomenon is described in the following paragraph.

It has been proposed that oxo-titanium species (superoxo- and hydroperoxo-titanium) are the reactive sites for olefin epoxidation reaction using H_2O_2 catalyzed by TS-1 [30,31]. The reactive oxo-titanium species in TS-1 was generated by interaction of tetrahedral titanium in TS-1 with aqueous H_2O_2 adducts. Therefore, the increase of epoxidation reaction rates in SZ/TS-1 catalysts can be explained by the rates of the formation of the reactive oxo-titanium species. The sulfate present on the surface of SZ/TS-1 probably can increase the adsorption rate of aqueous H_2O_2 onto TS-1. Consequently, the rate of the formation of oxo-titanium species increases and accordingly the production of epoxides is also increased. Meanwhile, a decrease in the activity of SZ/TS-1 samples that was observed at prolonged reaction time is probably due to the lower diffusion rate of 1-octene to the active sites inside the pore of TS-1.

The hydrolysis rate of 1,2-epoxyoctane to 1,2-octanediol using TS-1 loaded with sulfated zirconia using aqueous H_2O_2 as oxidant is shown in Fig. 8. Generally, TS-1, 15SZ/TS-1, 20SZ/TS-1 and TS-1-HZSM-5 were found to be active in the hydrolysis of 1,2-epoxyoctane although their activities are lower when compared with 20SZ/TS-1 and 15SZ/TS-1. Considering that SZ/TS-1 catalysts contain Brönsted acid sites, one expects that they are responsible for the hydrolysis of 1,2-epoxyoctane. Since the amount of Brönsted acid of 20SZ/TS-1 was higher than that of 15SZ/TS-1, its activity to hydrolyze 1,2-epoxyoctane was evidently higher as expected. It is noted that the amount of Brönsted acid in the TS-1-HZSM-5 was adjusted to be similar to that found in 20SZ/TS-1. However, the rate of the formation of 1,2-octanediol (up to 48 h) on the TS-1-HZSM-5 system was much lower and comparable with that on the low loading of SZ/TS-1 and TS-1. This indicates that highly active bifunctional oxidative and acidic catalyst may be prepared by deposition of SZ on the surface of TS-1 and cannot be achieved by mechanical mixing of TS-1 with HZSM-5.

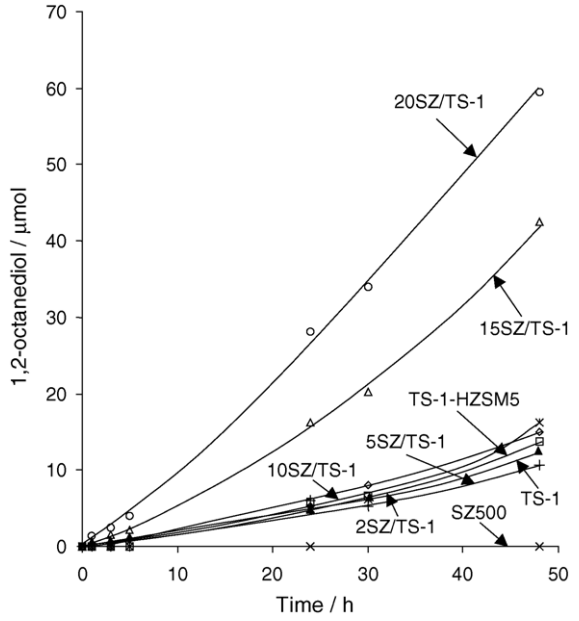

Fig. 8. The oxidation rate of hydrolysis of 1,2-epoxyoctane using TS-1 loaded with sulfated zirconia. All reactions were carried out in acetone as solvent at 70 °C.

Since the size of Zr^{4+} (ca. 0.1 nm), the source of SZ sites, is smaller than the size of the pore entrance of TS-1 (0.5 nm), the Zr species should be attached to the internal and external surfaces. As described in Section 3.5, it is possible that the SZ is located in a place where the silanol groups of TS-1 were previously positioned. Based on this consideration, it seems that SZ is effectively located close to Ti active sites, since the epoxide immediately reacts with SZ acid active site to hydrolyze the epoxide. This consecutive reaction is more difficult to occur efficiently over the TS-1-HZSM-5 catalytic system since the epoxide must diffuse to acid sites of HZSM-5 which are predominantly located in its pore. On the basis of these results, a model of the bifunctional oxidative and acidic catalytic system for consecutive reaction of 1-octene to 1,2-octanediol is proposed (see Fig. 9).

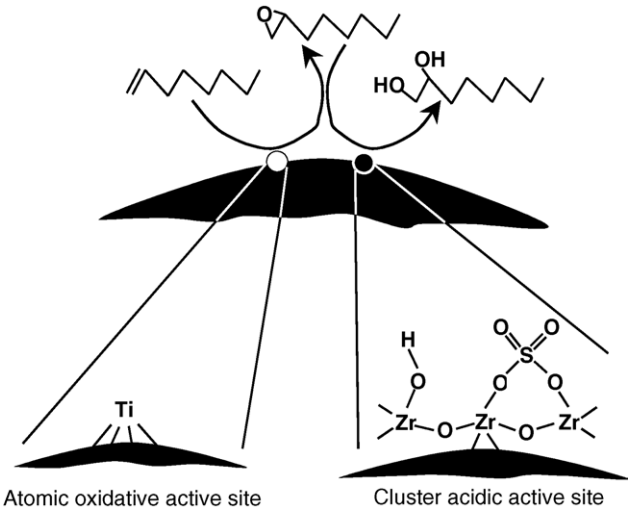

Fig. 9. Proposed model of TS-1 loaded with sulfated zirconia as bifunctional catalyst for consecutive transformation of 1-octene to 1,2-octanediol through the formation of 1,2-epoxyoctane.

4. Conclusion

Bifunctional oxidative and acidic catalysts have been successfully prepared by the dispersion of sulfated zirconia on the TS-1 at high zirconium loading up to double layer zirconium, i.e. 1.3 Zr^{4+} nm^{-2} TS-1. The catalysts have oxidative site due to titanium located in the framework of silicalite, while octahedral zirconium containing sulfate as Brönsted acidic sites. It has been demonstrated that samples with 15 and 20 wt% loadings of sulfated zirconia have shown the activity toward the consecutive transformation of 1-octene to 1,2-octanediol through the formation of 1,2-epoxyoctane using aqueous hydrogen peroxide.

Acknowledgement

We gratefully acknowledge funding from The Ministry of Science Technology and Innovation Malaysia (MOSTI), under IRPA grant no. 09-02-06-0057 SR0005/09-03.

References

[1] G. Centi, F. Cavani, F. Trifiro, in: M.V. Twigg, M.S. Spencer (Eds.), Fundamental and Applied Catalysis, Kluwer Academic Press, New York, 2001, p. 7.
[2] R.A. Sheldon, J. Dakka, Catal. Today 19 (1994) 215.
[3] M. Taramasso, G. Perego, B. Notari, US Patents No. 4,410,501 (1983).
[4] C. Perego, A. Carati, P. Ingallina, M.A. Mantegazza, G. Bellussi, Appl. Catal. A: Gen. 221 (2001) 63.
[5] M. Hino, S. Kobayashi, K. Arata, J. Am. Chem. Soc. 101 (1979) 6439.
[6] E.J. Hollstein, J.T. Wei, C.Y. Hsu, US Patent No. 4,918,041 (1990).
[7] B.H. Davis, R.A. Keogh, R. Srinivasan, Catal. Today 20 (1994) 219.
[8] C.Y. Hsu, V.K. Patel, D.H. Vahlsing, J.T. Wei, H.K. Myers Jr., US Patent 5,019,671 (1991).
[9] G.D. Yadav, J.J. Nair, Microporous Mesoporous Mater. 33 (1999) 1.
[10] S. Damyanova, P. Grange, B.J. Delmony, J. Catal. 168 (1997) 421.
[11] Y.Y. Huang, B.Y. Zhao, Y.C. Xie, Appl. Catal. A: Gen. 173 (1998) 27.
[12] T. Lei, J.S. Xu, Y. Tang, W.M. Hua, Z. Gao, Appl. Catal. A: Gen. 192 (2000) 181.
[13] C.L. Chen, C. Tao, L. Soofin, P. Hong, C.J. Bhongale, C.Y. Mou, Microporous Mesoporous Mater. 50 (2001) 201.
[14] I.J. Dijs, J.W. Geus, L.W. Jenneskens, J. Phys. Chem. B 107 (2003) 13403.
[15] J.R. Sohn, D.H. Seo, Catal. Today 87 (2003) 219.
[16] A.J.H.P. van der Pol, A.J. Verduyn, J.H.C. van Hooff, Appl. Catal. A: Gen. 92 (1992) 113.
[17] E.M. Flanigen, in: J.A. Rabo (Ed.), Zeolite Chemistry and Catalysis, vol. 171, ACS Monograph, 1976, p. 80.
[18] K.S. Smirnov, B. van de Graaf, Microporous Mater. 7 (1996) 133.
[19] E. Astorino, J.B. Peri, R.J. Willey, G. Busca, J. Catal. 157 (1995) 482.

[20] G. Ricchiardi, A. Damin, S. Bordiga, C. Lamberti, G. Spano, F. Rivetti, A. Zecchina, J. Am. Chem. Soc. 123 (2001) 11409.
[21] S. Bordiga, A. Damin, F. Bonino, A. Zecchina, G. Spano, F. Rivetti, V. Bolis, C. Prestipino, C. Lamberti, J. Phys. Chem. B 106 (2002) 9892.
[22] B. Rakshe, V. Ramaswamy, S.G. Hegde, R. Vetrivel, A.V. Ramaswamy, Catal. Lett. 45 (1997) 41.
[23] B.Q. Xu, W.M.H. Sachtler, J. Catal. 167 (1997) 224.
[24] R. Srinivasan, R.A. Keogh, D.R. Milburn, B.H. Davis, J. Catal. 153 (1995) 123.
[25] I.V. Bobricheva, I.A. Stavitsky, V.K. Yermolaev, N.S. Kotsarenko, V.P. Shmachkova, D.I. Kochubey, Catal. Lett. 56 (1998) 23.
[26] C.R. Vera, C.L. Pieck, K. Shimizu, J.M. Parera, Appl. Catal. A: Gen. 230 (2002) 137.
[27] D.J. Rosenberg, B. Bachiller-Baeza, T.J. Dines, J.A. Anderson, J. Phys. Chem. B 107 (2003) 6526.
[28] J.R. Sohn, W.C. Park, Appl. Catal. A: Gen. 239 (2003) 269.
[29] A. Clearfield, G.P.D. Serrette, A.H. Khazi-Syed, Catal. Today 20 (1994) 295.
[30] D. Srinivas, P. Manikandan, S.C. Laha, R. Kumar, P. Ratnasamy, J. Catal. 217 (2003) 160.
[31] F. Bonino, A. Damin, G. Ricchiardi, M. Ricci, G. Spano, R. D'Aloisio, A. Zecchina, C. Lamberti, C. Prestipino, S. Bordiga, J. Phys. Chem. B 108 (2004) 3573.